
DESIGN, ANALYSIS AND EXPERIMENTAL VERIFICATION OF A NOVEL NONLINEAR PI CONTROLLER

Şirin AKKAYA¹, Handan NAK¹, Ali Fuat ERGENÇ^{1,*}

¹ Control and Automation Engineering, Faculty of Electrical and Electronical Engineering, Istanbul Technical University, Istanbul, Turkey

ABSTRACT

In this study, a novel variable gain PI controller structure is introduced. The proposed controller structure consists of a sector-bounded nonlinear function of the relative error value in cascade with a linear fixed-gain PI controller. The stability analysis of the closed loop system is examined through Popov stability criterion, Routh-Hurwitz stability method and stability boundary locus method for both second-order and higher-order systems. In addition, the performance of the controller against parameter variations and disturbances is investigated through some simulations for second order systems. An experimental study, an active suspension system, is conducted to examine the performance of the controller for higher order systems. In the literature, there are similar controllers, but the proposed one is superb in terms of effectiveness and stability. The new controller prevents the saturation of the controller signal. Simulation results and experimental studies reveal that proposed controller structure is quite effective for both lower and higher order systems.

Keywords: Nonlinear PI, Variable gain, Popov criterion, Stability boundary locus, Active suspension.

1. INTRODUCTION

In several decades, numerous new and powerful methodologies are developed in the field of control engineering, however, conventional PID and PI type controllers are most popular among these structures especially in the industrial control systems. The main motivation behind this choice is the simplicity of the structure of controller and their unquestionable stability properties.

Generally, the expectation from the control system is that the controlled system has fast response, no steady state error with small overshoot, as well as robust performance against parameter uncertainties and disturbances. A constant disturbance to the system may be rejected utilizing an integral term in the controller, but it is known fact that this term introduces undesired increase of the system overshoot [1, 2]. Remedy of this contradiction, nonlinear variable gain controller structures are proposed to diminish steady state error due to disturbances, while maintaining acceptable overshoot levels and system speed [3, 4]. In the literature, there are quite a few studies on such nonlinear variable gain controllers for linear systems to improve the controller performances [5-10]. In [5], Hunnekens *et al.* proposed a variable gain integral controller to improve transient performance of linear motion systems. They focused on tradeoff introduced by integral action. They also proposed an optimization strategy, which enables performance optimal tuning of the variable gain. Armstrong *et al.* proposed a nonlinear PID controller as a function of system state. They extended their previous studies [6-8] to tracking and to systems with state feedback and integral control [9]. In [10], authors designed a nonlinear filter based on Lyapunov arguments to improve nanopositioning servo performances in high-speed motion systems. They demonstrated proposed structure on a short-stroke wafer stage of an industrial wafer scanner. A method for the performance assessment of a variable-gain control design for optical storage drives is proposed in [11] to overcome well-known linear control design trade-offs between low-frequency tracking properties and high-frequency noise sensitivity.

*Corresponding Author: ali.ergenc@itu.edu.tr

The main goal of this study is to modulate several or all the controller coefficients to enhance the controller performance. A nonlinear gain, which is associated in series with a constant coefficient linear controller, is employed to achieve this goal. The function of the nonlinear gain is generally preferred as a sigmoid, hyperbolic or fractional-linear function of the error [12, 13].

One of the key components of the design of variable coefficient controllers is to assess the stability of the system with respect to the variation of nonlinear gain. In literature, Popov stability criterion and Lyapunov method are employed for this purpose. The stability analysis using the Popov stability criterion of nonlinear P, PD, PI and PID controllers on a simple robotic system with second-order dynamics has been extensively discussed in [14] and similar analyses have been investigated in different studies [15, 16]. In these analyses, the systems are considered as Lure type of system. The proposed nonlinear controller was handled as an independent sector-bounded nonlinear function and the stability analysis presents a range of the sector, in other words, the range of the variation of nonlinear gain. In [17] and [18], the Lyapunov method is employed for the stability analysis. The total energy of the system including the controller is considered as the descriptive Lyapunov function and it is proven that when the controller satisfies certain conditions, the derivative of the Lyapunov function is non-positive.

The main contribution of this study is a new nonlinear gain feature which is not only function of the error but also reference signal. In this scheme, the gain increases with a function of the error relative to the reference, thus the control signal increases exponentially, and similarly, decrease in relative error results an exponential decrease in control signal. This novel gain structure of the controller has two advantages. First advantage is an exponential change in proportional term, which facilitates controller to apply a strong control action to decrease the rise time of the system response. Second advantage is in integral term effect of the controller. Exponential decrease of integral action when error reaches to zero inarguably prevents overshoot of the system response compared to fixed-gain integral controller. The combination of these two improved actions represents a novelty in PID controllers.

Another aspect of the nonlinear gain function, which presents a key advantage against the similar approaches in the literature, is that the function is a sigmoid type which limits the nonlinear gain thus the control signal. The stability analysis of this controller is elaborated for second and higher order systems, respectively. A basic mass-spring-damper system is considered as a second order system, and a fourth-order active suspension system as a higher order system. Moreover, the experiments are conducted using the active suspension benchmark developed by Quanser[®] Company.

Three different stability analysis method are utilized for both systems; Popov stability criterion, Routh-Hurwitz stability criterion and stability boundary locus method. The stable range of the sector of nonlinear variation is obtained utilizing the Popov stability criterion. The nonlinear function is considered as a variable gain and the stable range of the gain is determined via the Routh-Hurwitz stability method. The stability boundary locus method provided the stability locus on the k_p - k_i plane [19, 20]. All three stability analysis revealed the same results for each type of system.

The paper is organized as follows; the proposed method is described in Section 2. In Section 3, the stability analysis for the second order mass-spring-damper system with the controller is studied using Popov stability criterion, Routh-Hurwitz criterion and stability boundary locus method, respectively. The section is concluded with the simulation results. In Section 4, the active suspension system is introduced; the stability analysis is inspected using all three methods, followed by the simulation results. The results of the experimental study are presented in Section 5. The conclusion remarks are in Section 6.

2. CONTROLLER STRUCTURE

The mathematical description of a fixed-gain PI controller is generally expressed as follows

$$u(t) = k_p e(t) + k_i \int_0^t e(t) dt \quad (1)$$

where $u(t)$ is control signal, $r(t)$ is system reference, $y(t)$ is system output, $e(t)$ is error signal, and k_p and k_i are constant proportional and integral gains, respectively.

The proposed control structure consists of a nonlinear gain $k(e,r)$ which is placed in cascade with a fixed-gain PI controller in Equation 1, as in Equation 2. The block diagram of the proposed structure is illustrated in Figure 1.

$$u(t) = \left[k_p e(t) + k_i \int_0^t e(t) dt \right] k(e) \quad (2)$$

In previous studies, the nonlinear gain $k(e)$ is defined as a nonlinear function of only the error signal $e(t)$, and it is bounded in an interval $[k(e)_{min}, k(e)_{max}]$. The proposed a novel nonlinear gain function $k(e,r)$ is defined as

$$k(e,r) = \gamma - \alpha e^{-\beta\delta} \quad (3)$$

where $\delta = |e(t)/r(t)|$ and, α , β and γ are positive-valued controller design parameters. Note that, the $k(e,r)$ function is bounded in $[\gamma - \alpha, \gamma]$ with this definition.

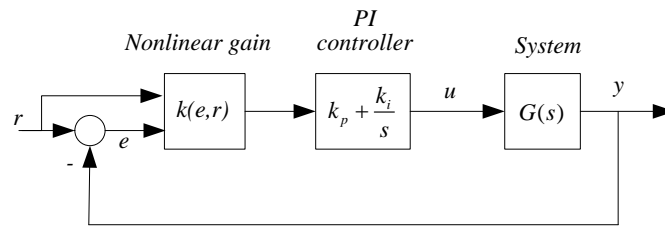


Figure 1. Nonlinear PI control system block diagram.

In the proposed control structure, the error signal is amplified with a term, which is defined by the ratio of error to the reference and fed into fixed-gain controller. Thus, a rapid change in the reference results in a larger relative error. Consequently, the exponential term verge on zero and the pre-controller signal is amplified by approximately γ times of the error. In other words, when the relative error value is large, controller gains exponentially increase and the controller drives the system output to the reference value rapidly. On the hand, when the relative error value tends to decrease, the controller coefficients exponentially decrease and nonlinear gain $k(e,r)$ approximates to the lowest value $(\gamma - \alpha)$ when the error vanishes. In essence, the controller behaves as an aggressive controller with higher controller parameters for large error, and a moderate controller with smaller controller parameters for small error, which shortens the rise time and allows the system output behavior being smoother in the process of settling when compared to the fixed-gain PI controller.

The major modification of this controller structure from the other nonlinear controller structures in the literature is the variation of the nonlinear gain with the reference value. In this way, the control signal is proportionally generated to the relative error, which has positive effect on system response. Meanwhile, the decrease of the error is translated in an exponential decrease in the control signal and this effectively prevents the system from overshoot. This structure also reduces the winding of the integral term, which is another cause of overshoot.

3. CONTROL OF SECOND ORDER SYSTEM

In many physical applications, system dynamics are generally modelled by second order differential equations. Besides it is possible to express higher order systems with second order dynamic equations formed by dominant complex roots of original system [14]. In order to understand the main idea behind the proposed controller structure and analyze the stability, a second order mass-spring-damper system given in Figure 2 is preferred. Here, m , k and b represent mass, spring constant and damping constant, respectively. The transfer function between the applied force (system input), $F(s)$, and position (system output), $X(s)$, is presented in Equation 4.

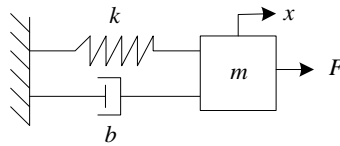


Figure 2. The schematic of second-order mass-spring-damper system.

$$\frac{X(s)}{F(s)} = \frac{1}{m s^2 + b s + k} \tag{4}$$

The stability analysis of the closed loop unit feedback system with the proposed controller is studied utilizing Popov stability criterion, stability boundary locus method [19] and Routh-Hurwitz stability criterion. The outcome of these three tests coincided.

3.1. Popov Stability Criterion

The Popov stability criterion is used for the stability analysis of the variable coefficient PI control system with sector-bounded nonlinear gain that connected in series to the stable, linear fixed-gain PI control system as in [14, 21]. The Popov criterion states a sufficient condition for the closed loop system to be globally asymptotic stable for all nonlinear gains in the sector $0 \leq k(e) \leq k(e)_{max}$. This means that the Popov plot of $W(j\omega)$ which is the forward transfer function of the linear part of the system, lies entirely on the right of a straight line with a nonnegative slope passing through the point $1/k(e)_{max}$ [14].

The linear part of the open loop transfer function for the system is given in Equation 5.

$$W(s) = \frac{k_i + k_p s}{s(m s^2 + b s + k)} \tag{5}$$

The crossing point of the Popov plot of the $W(j\omega)$ with the real axis should be obtained for the application of the Popov stability criterion. The real and imaginary part of the $W(j\omega)$ is given in Equation 6.

$$\begin{aligned}
 \operatorname{Re}(W(j\omega)) &= \frac{-(k_p m \omega^2 + b k_i - k k_p)}{b^2 \omega^2 + (k - m \omega^2)^2} \\
 \omega I_m(W(j\omega)) &= \frac{-[(b k_p - k_i m) \omega^2 + k k_i]}{b^2 \omega^2 + (k - m \omega^2)^2}
 \end{aligned}
 \tag{6}$$

The Popov plot of the $W(j\omega)$ starts from $P(-(b k_i - k k_p)/k^2, -k_i/k)$ for $\omega=0$, and end at $Q(0, 0)$ for $\omega=\infty$. Here, depending on the k_p and k_i values, two cases are possible. In the case of $k_i \leq (b/m)k_p$, the $\omega I_m W(j\omega)$ term is always negative regardless of the ω values and the Popov plot of the $W(j\omega)$ always remains in the third and fourth quadrants of the complex plane, which means the plot does not cross the real axis. Therefore, one can plot a straight line passing through the origin with nonnegative slope while the Popov plot of $W(j\omega)$ entirely lies on the right of that line.

In the case of $k_i > (b/m)k_p$, the Popov plot of the $W(j\omega)$ crosses in the real axis and the cut-off frequency and the crossing point is given in Equation 7 and 8, respectively.

$$\omega_0^2 = \frac{k k_i}{k_i m - b k_p}
 \tag{7}$$

$$\operatorname{Re}(W(j\omega_0)) = \frac{b k_p - k_i m}{b k}
 \tag{8}$$

The Equation 8 reveals that the Popov plot of the $W(j\omega)$ crosses into negative real axis, and here, the maximum nonlinear coefficient value is obtained as

$$k(e, r)_{\max} = -\frac{1}{\operatorname{Re}(W(j\omega_0))} = \frac{-b k}{b k_p - k_i m}
 \tag{9}$$

In both cases, the graphical results are given in Figure 3, for $m = 0.01$ kg, $b = 0.03$ Nsec/m, $k = 1$ N/m, $k_p = 10$, $k_i = 15$ (for case (a)) and $k_i = 100$ (for case (b)).

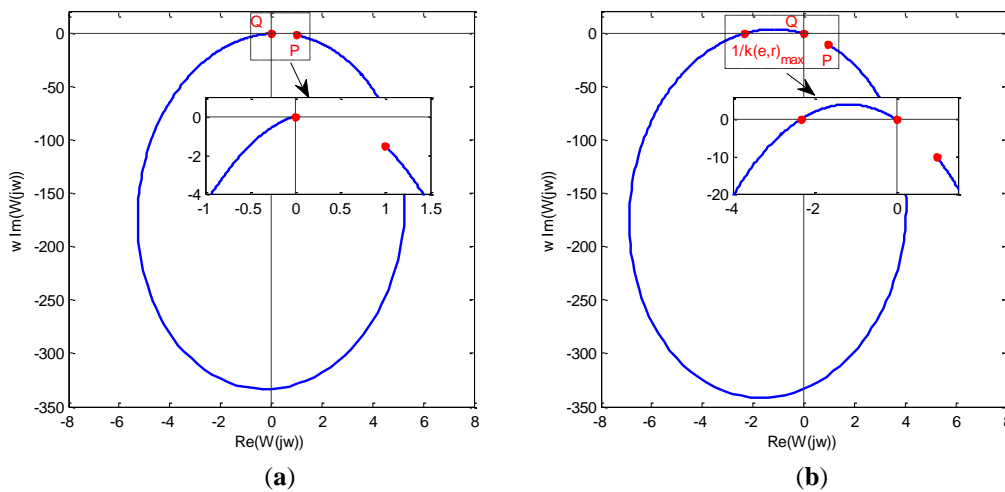


Figure 3. The Popov plot of the $W(j\omega)$ (a) the case of $k_i \leq (b/m)k_p$ (b) the case of $k_i > (b/m)k_p$.

3.2. Routh-Hurwitz Stability Criterion

The stability of closed loop system is examined by using Routh Hurwitz stability criteria. In this method, the boundaries of nonlinear gain $k(e,r)$ are determined by considering that gain $k(e,r)$ is a fixed parameter.

The closed loop system transfer function with proposed control structure is given in Equation 10.

$$T(s) = \frac{k(e,r)(k_i + k_p s)}{k(e,r)k_i + ks + k(e,r)k_p s + bs^2 + ms^3} \quad (10)$$

Routh table generated according to the characteristic equation of closed loop system in Equation 10 and based on the criterion, it is said that $k(e,r)$ gain must satisfy the following conditions so that the system is stable:

Condition 1: $k_i > 0$ and if $k_i \leq \frac{b}{m}k_p$, then $k(e) > 0$.

Condition 2: $k_i > 0$ and if $k_i > \frac{b}{m}k_p$, then $0 < k(e) \leq \frac{-bk}{bk_p - k_i m}$.

It should be noted that both stability analysis provide same results.

3.3. Stability Boundary Locus Method

This method is proposed for computation of stabilizing PI controllers in the $k_i - k_p$ parameter plane [18, 19]. Here, the problem is to compute the parameters of PI controllers which stabilize the system given Figure 1 with the nonlinear gain $k(e,r)$ that is considered as a fixed gain. So, nonlinear PI controller becomes

$$C(s) = \frac{k_i^* + k_p^* s}{s} \quad (11)$$

where $k_i^* = k(e,r)k_i$ and $k_p^* = k(e,r)k_p$.

The closed loop characteristic polynomial of the system that obtained by substituting $s = j\omega$ is written as

$$\Delta(j\omega) = Re_\Delta + Im_\Delta \quad (12)$$

where $Re_\Delta = k_i^* - b\omega^2$ and $Im_\Delta = k\omega + k_p^* \omega + m\omega^3$

Then, equating the real and imaginary parts of $\Delta(j\omega)$ to zero, one obtains the following equation for k_p^* and k_i^* .

$$\begin{aligned} k_i^* &= b\omega^2 \\ k_p^* &= -k + m\omega^2 \end{aligned} \quad (13)$$

The stability boundary locus is obtained in the $k_i - k_p$ plane by solving the equations given Equation 13. The stability boundary locus and the line $k_i^* = 0$ divide the parameter plane into stable and unstable regions [20]. Following the partition, to determine the stability region, each region in the $k_i - k_p$ plane

should be tested by picking a point in the set and checking the stability of the closed loop system. In Figure 4(a) the parametric stability boundary locus of a second order system with a PI controller in (11) is depicted.

For a (k_i, k_p) pair that located in the stability region, k_i^* and k_p^* values lie on a straight line passing through the (k_i, k_p) pair and origin (for $k(e, r) = 0$). The crossing maximum $k(e, r)$ values is evaluated from the intersection point between the straight line and the stability locus. k_i must be positive to guarantee the stability, which forces the minimum value of $k(e, r)$ to be zero.

To compare the stability boundary locus with the results of other stability criteria, one can divide the stability region into two parts shown as Figure 4 (b). The parts of the stability region correspond to case 1 and case 2 that explained in Popov and Routh-Hurwitz stability criterion sections.

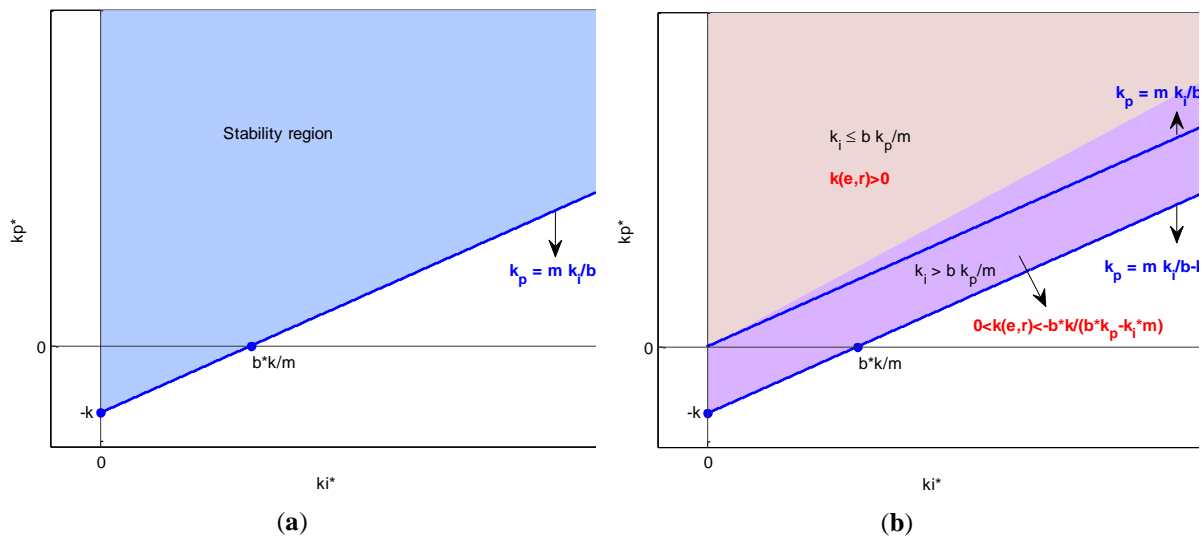


Figure 4. (a) The whole stability region of the system (b) the part of the stability region that correspond to case 1 and 2.

In the last step, it is necessary to define the boundaries of the parameters α , β and γ of the nonlinear gain expression given in Equation 3, which satisfy condition 1 and condition 2. It is obvious that the boundaries for $k(e, r)$ in conditions correspond to the boundaries of nonlinear gain function that is given earlier. When both conditions are examined, it is seen that there is no constraint for β parameter for stability point of view, but following inequalities depending on α and γ parameters should be satisfied.

Condition 1: $k_i > 0$ and if $k_i \leq \frac{b}{m} k_p$, then $\alpha < \gamma$.

Condition 2: $k_i > 0$ and if $k_i > \frac{b}{m} k_p$, then $\gamma < \frac{-bk}{bk_p - k_i m}$ and $\alpha < \gamma$.

3.4. Simulation Studies

A second order mass-spring-damper system (see Figure 2) is controlled using the proposed controller in order to test the performance. The simulation diagram in Figure 5 is constructed in Matlab/ Simulink[®], and performance of proposed nonlinear PI controller is compared with a fixed-gain PI controller which has same controller parameters k_p and k_i . The parameters in simulation are given in Table 1. Note that with these system parameters and controller parameters including α and γ are in stable region.

Table 1. Simulation parameters

Parameter	Value
Mass, m	2.45 kg
Damping coefficient, b	18 Nsec/m
Spring constant, k	400 N/m
Proportional gain, k_p	25
Integral gain k_i	150
Controller parameter, α	0.4
Controller parameter, β	1
Controller parameter, γ	2

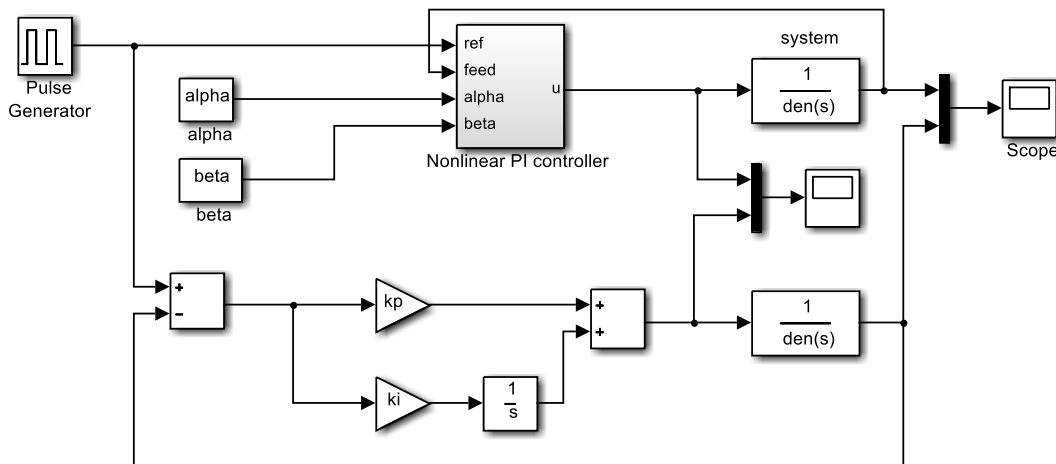


Figure 5. Simulation diagram constructed in Matlab/Simulink.

In the simulations, a square wave with a frequency of 0.0125 Hz and amplitude 1 is utilized as the reference signal. The results are presented in Figure 6 and 7. In Figure 6, it is visible that the proposed structure accelerates the system response compared with the fixed-gain PI controller. When reference signal changes, the relative error reaches high values, and as visible in Figure 7, $k(e, r)$ gain increases. Similarly, when the output value approaches the reference, the error decreases and nonlinear $k(e, r)$ gain decreases as expected. Note that for zero reference, since relative error term, δ goes to infinity, a small epsilon term is added to the denominator of δ , such that $= |e(t)/(r(t) + \epsilon)|$. Here ϵ is selected as 0.001. The proposed controller increases the performance of the classical controller without any overshoot.

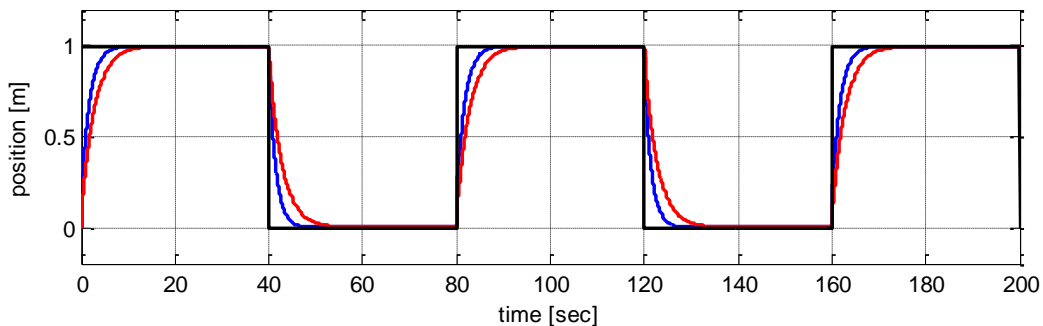


Figure 6. System response for nonlinear and fixed-gain PI controllers. Nonlinear PI controller response in blue line, fixed-gain PI controller response in red line, reference in black line.

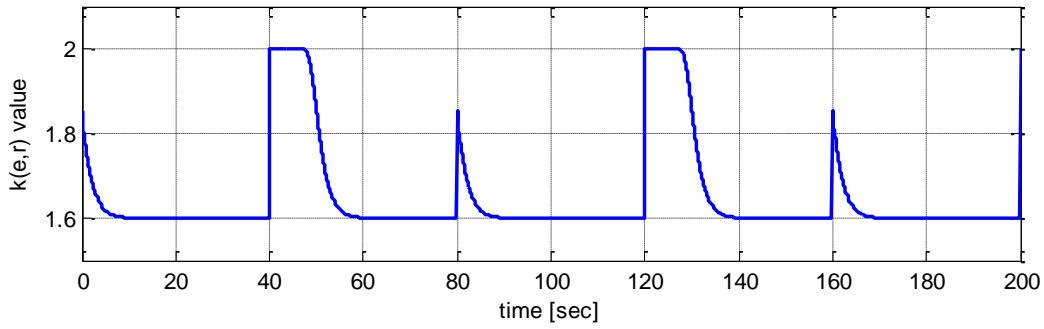


Figure 7. Variation of nonlinear gain $k(e,r)$ with respect to time.

The disturbance rejection performance of proposed controller is investigated by introducing a step disturbance input with the amplitude of 0.5 at $t=20$ s. The result of this case is in Figure 8. Accordingly, it is clear that nonlinear PI controller performs better both reference tracking and disturbance rejection.

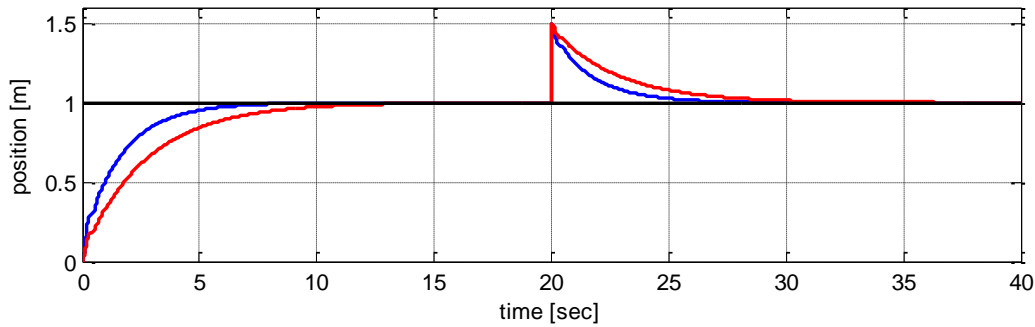


Figure 8. The output disturbance rejection response of the nonlinear PI and fixed-gain PI control system. Nonlinear PI controller response in blue line, PI controller response in red line, reference in black line.

Figures 9, 10 and 11 illustrate the effect of controller parameters α , β and γ on controller performance, respectively. Though the system response accelerates when the α parameter is decreased within the stability limits, the system response slows down when the β parameter is decreased. For higher values of the γ parameter, system response becomes more aggressive.

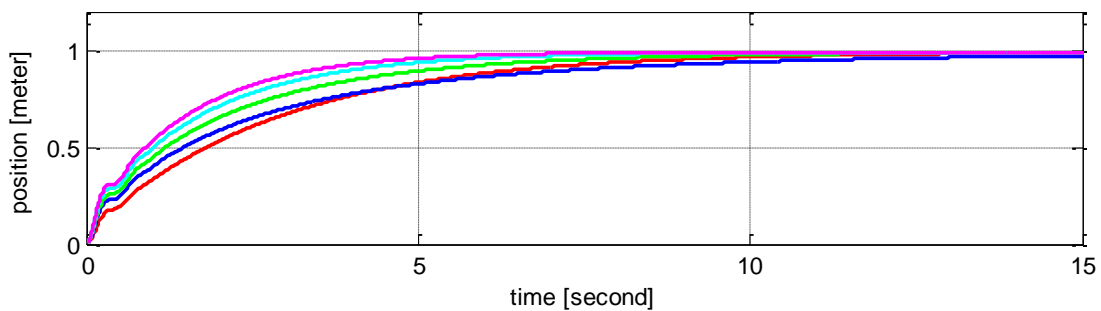


Figure 9. The controller performance for different α parameters. Fixed-gain PI controller response in red line, $\alpha=1.5$ in blue line, $\alpha=1$ in green line, $\alpha=0.5$ in cyan line, $\alpha=1.5$ in magenta line ($\beta=1$ and $\gamma=2$).

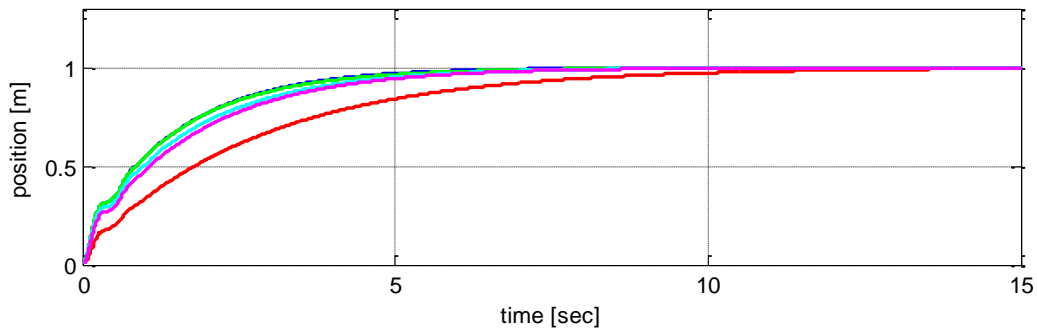


Figure 10. The controller performance for different β parameters. Fixed-gain PI controller response in red line, $\beta=100$ in blue line, $\beta=10$ in green line, $\beta=1$ in cyan line, $\beta=0.1$ in magenta line ($\alpha=0.5$ and $\gamma=2$).

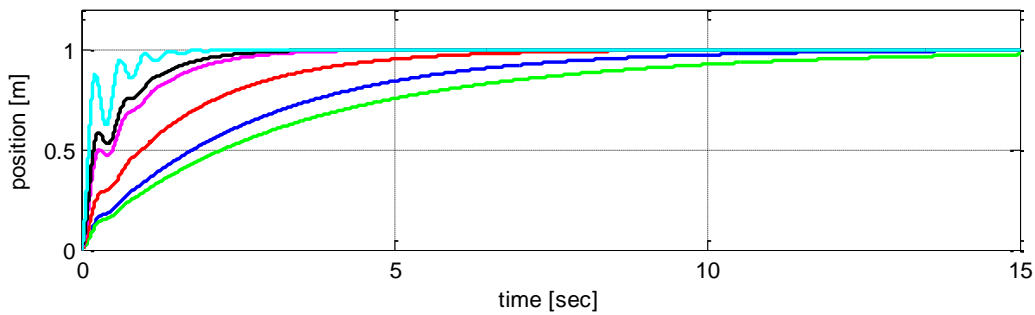


Figure 11. The controller performance for different γ parameters. Fixed-gain PI controller response in blue line, $\gamma=1$ in green line, $\gamma=2$ in red line, $\gamma=4$ in magenta line, $\gamma=5$ in black line, $\gamma=10$ in cyan line ($\alpha=0.4$ and $\beta=1$).

Finally, performance of proposed controller is tested by changing the system parameters given in Table 1. The system responses in Figure 12 shows that proposed controller is more robust than the fixed-gain PI controller against parameter variations.

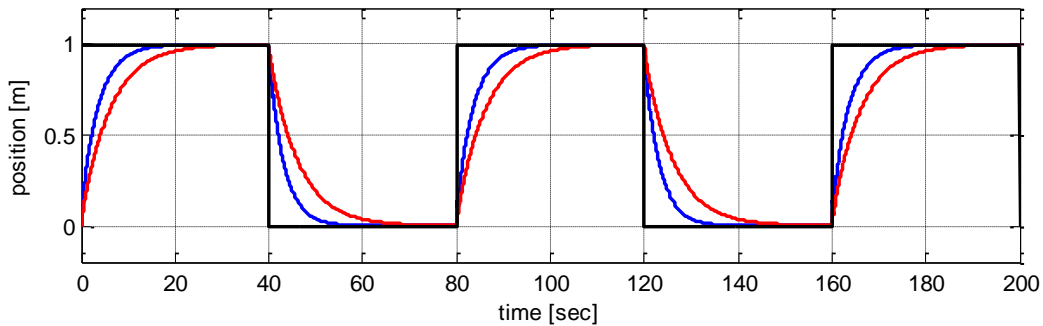


Figure 12. System responses for $b=7.5$ and $k=900$. Nonlinear PI controller response in blue line, fixed-gain PI controller response in red line, reference in black line.

4. CONTROL OF HIGHER ORDER SYSTEMS

In this section, as a higher order system, we examine a vehicle active suspension control system. In active suspension systems, the passive force elements are accompanied by active force elements. The objective of control is to improve the ride comfort and handling ability under different road conditions.

An active suspension system on a quarter-car model is schematically illustrated in Figure 13. The system consists of two masses; mass of the vehicle body, M_s and mass of tire, M_{us} . A spring and a damper support each mass. The spring K_s and the damper B_s support the body weight over the tire, while the spring K_{us} and the damper B_{us} represent the stiffness and damping properties of the tire in contact with the road. The generalized coordinate x_1 represents the tire displacement and x_2 represents the vehicle body displacement all with respect to the ground. The system has two external inputs, road surface position z_r and control force F_c .

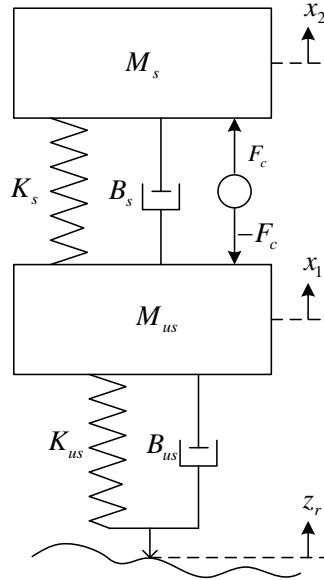


Figure 13. Double mass-spring-damper model for active suspension system [22].

Governing equations of motion, where all the initial conditions are assumed zero, are obtained as below.

$$\begin{aligned} \ddot{x}_2 &= -g + \frac{F_c}{M_s} + \frac{B_s \dot{x}_1}{M_s} - \frac{B_s \dot{x}_2}{M_s} + \frac{K_s x_1}{M_s} - \frac{K_s x_2}{M_s} \\ \ddot{x}_1 &= -g - \frac{F_c}{M_{us}} - \frac{(B_s + B_{us}) \dot{x}_1}{M_{us}} + \frac{B_s \dot{x}_2}{M_{us}} + \frac{B_{us} \dot{z}_r}{M_{us}} - \frac{(K_s + K_{us}) x_1}{M_{us}} + \frac{K_s x_2}{M_{us}} + \frac{K_{us} z_r}{M_{us}} \end{aligned} \quad (14)$$

The gravitational force only changes the equilibrium point of the positions in the equations of motion and it has no effect on the dynamics of the system. For omitting gravity forces from the equations of motion, the following change of variables to the equations of motion is applied. In other words, the relaxed position of the springs, i.e. $z_{us}=0$, $z_s=0$, will be the equilibrium point of the system [22].

$$x_1 = z_{us} - \frac{g(M_s + M_{us})}{K_{us}}, \quad x_2 = z_2 - \frac{gM_s}{K_s} - \frac{g(M_s + M_{us})}{K_{us}}, \quad (15)$$

Following the transformation, the equations of motion turn into:

$$\begin{aligned} M_{us} \ddot{z}_{us} &= -B_s \dot{z}_{us} - B_{us} \dot{z}_{us} - F_c + B_s \dot{z}_s + B_{us} \dot{z}_r - (z_{us} - z_s) K_s - (z_{us} - z_s) K_{us} \\ M_s \ddot{z}_s &= B_s \dot{z}_{us} + F_c + B_s \dot{z}_s - (z_s - z_{us}) K_s \end{aligned} \quad (16)$$

In our approach, the active suspension control command F_c is the control signal, and road surface velocity \dot{z}_r , also represents road roughness, is regarded as the disturbance signal. The aim of control is to ensure that vehicle body position, z_s tracks the road position, z_r with minimum vibration. Using Equation 16, the transfer function between vehicle body velocity and disturbance signal, and also, the transfer function between vehicle body position and control command are obtained as follows;

$$L\left(\frac{\dot{z}_s}{\dot{z}_r}\right) = \frac{B_s B_{us} s^2 + (K_s B_{us} + K_{us} B_s) s + K_s K_{us}}{M_s M_{us} s^4 + (M_s B_{us} + B_s M_{us} + M_s B_s) s^3 + (M_s K_{us} + B_s M B_{us} + M_s K_s + M_{us} K_s) s^2 + (K_s B_{us} + B_s K_{us}) s + K_s K_{us}} \quad (17)$$

$$L\left(\frac{z_s}{F_c}\right) = \frac{M_{us} s^2 + B_{us} s + K_{us}}{M_s M_{us} s^4 + (M_s B_{us} + B_s M_{us} + M_s B_s) s^3 + (M_s K_{us} + B_s M B_{us} + M_s K_s + M_{us} K_s) s^2 + (K_s B_{us} + B_s K_{us}) s + K_s K_{us}}$$

In the following parts of the study, the transfer function between vehicle body position and control command is employed. The stability analysis of the given system is examined by three methods as discussed in Section 3. However, since the transfer function is fourth order, analyzing the closed loop system stability with proposed control structure with parametric transfer function is quite complicated. Therefore, we consider the active suspension system with numeric values of system parameters, which are evaluated in Table 2.

Table 2. Active suspension system parameters.

Parameter	Value
Vehicle body mass, M_s	2.45 kg
Tire mass, M_{us}	1 kg
Suspension stiffness, K_s	900 N/m
Tire stiffness, K_{us}	1250 N/m
Suspension damping coefficient, B_s	7.5 Nsec/m
Tire damping coefficient, B_{us}	5 Nsec/m

By substituting the system parameters, the numerical transfer function is obtained as

$$\frac{z_s(s)}{F_c(s)} = \frac{s^2 + 5s + 1250}{2.45s^4 + 38.125s^3 + 6205s^2 + 13875s + 1125000} \quad (18)$$

PID type controller is employed to suppress the vibrations of the active suspension system more effectively. Therefore, to separate the PI part of controller from the whole plant, vehicle suspension system in Equation 18 and PD controller is considered, which is connected in series with the suspension system, as a new system to be controlled. A PD type controller with proportional gain 1 and derivative gain 5, one can obtain the transfer function of the cascade system as

$$\frac{z_s(s)}{F_c(s)} = \frac{5s^3 + 26s^2 + 62555s + 1250}{2.45s^4 + 38.125s^3 + 6205s^2 + 13875s + 1125000} \quad (19)$$

From now on, we study the stability of the system in Equation 19.

4.1. Popov Stability Criterion

To investigate the absolute stability of the closed loop system in Figure 1 with Popov criterion, it is necessary to compute the linear part of open loop transfer function of the control system, and divide its frequency response into real and imaginary parts as follows

$$W(s) = \frac{(k_p s + k_i)(5s^3 + 26s^2 + 6255s + 1250)}{s(2.45s^4 + 38.125s^3 + 6205s^2 + 13875s + 1125000)} \quad (20)$$

$$\text{Re}(W(j\omega)) = \frac{k_i(7.02 \times 10^9 - 4.4 \times 10^7 \omega^2 + 43358 \omega^4 - 12.5 \omega^6) + k_p(1.4 \times 10^9 + 4.98 \times 10^7 \omega^2 - 14345.4 \omega^4 + 126.9 \omega^6)}{1.26 \times 10^{12} - 1.37 \times 10^{10} \omega^2 + 4.3 \times 10^7 \omega^4 - 28951 \omega^6 + 6 \omega^6} \quad (21)$$

$$\omega \text{Im}(W(j\omega)) = \frac{k_i(-1.4 \times 10^9 - 4.98 \times 10^7 \omega^2 + 14345.4 \omega^4 - 126.9 \omega^6) + k_p \omega^2(7.02 \times 10^9 - 4.4 \times 10^7 \omega^2 + 43358 \omega^4 - 12.5 \omega^6)}{1.26 \times 10^{12} - 1.37 \times 10^{10} \omega^2 + 4.3 \times 10^7 \omega^4 - 28951 \omega^6 + 6 \omega^6}$$

In this case, examining the Popov plot of $W(j\omega)$, it is not straightforward as it is in Section 3. Therefore, we choose some test points for k_p and k_i to plot the curve and find the crossing point of real axis. For example, the Popov plot is obtained for $k_p = -0.25$ and $k_i = 500$ (see Figure 14(a)) and for $k_p = 12$ and $k_i = 150$ (see Figure 14 (b)).

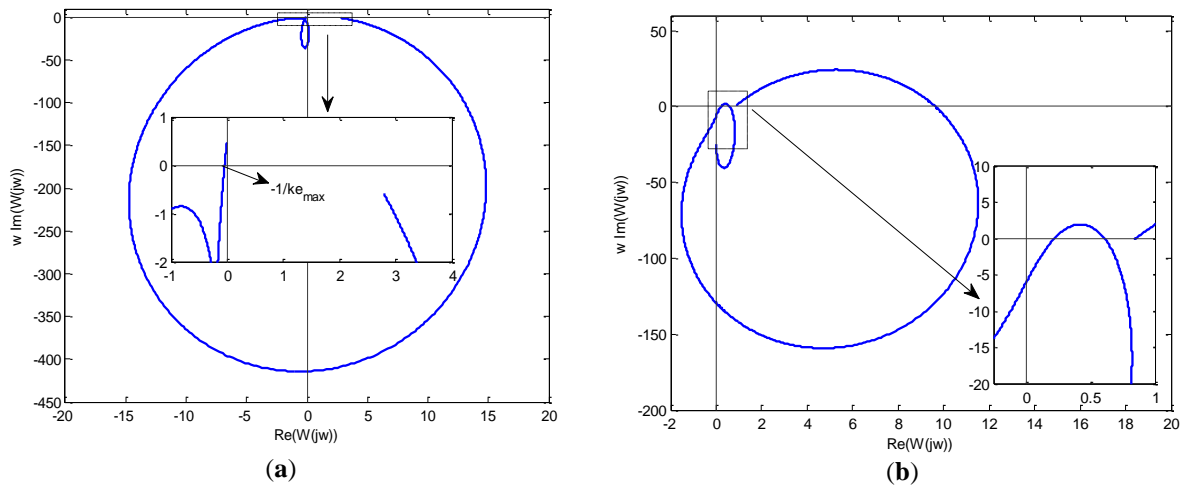


Figure 14. (a) Popov plot for $k_p = -0.25$ and $k_i = 500$ (b) Popov for $k_p = 12$ and $k_i = 150$.

In Figure 14(a) the Popov plot of $W(j\omega)$ crosses the real axis. The crossover frequency and crossover point may be obtained by using Equation 21. Then, the maximum value of nonlinear gain $k(e,r)$ is equal to the negative reciprocal of the crossing point (in this case it is equal to 21.5675) as mentioned in Section 3.1. Thus the range of nonlinear gain $k(e,r)$ is determined as $(0, 21.5675)$. In Figure 14(b) the Popov plot of $W(j\omega)$ remains entirely in the first, third and fourth quadrants and does not cross the negative real axis. A straight line with a nonnegative slope passing through the origin may be built that is located entirely on the left of the Popov plot. Hence, the range of nonlinear gain $k(e,r)$ is found as $(0, \infty)$.

As a result, it is possible to determine the range of nonlinear gain $k(e,r)$ numerically by using this stability criterion for fixed-valued controller parameters k_i and k_p to control the vehicle active suspension system.

4.2. Routh-Hurwitz Stability Criterion

The characteristic equation of the vehicle active suspension control system with proposed control structure is as in Equation 22:

$$\Delta(s) = 2.45s^5 + (5k(e,r)k_p + 38.125)s^4 + (26k(e,r)k_p + 5k(e,r)k_i + 6205)s^3 + (26k(e,r)k_i + 6255k(e,r)k_p + 13875)s^2 + (1250k(e,r)k_p + 6255k(e,r)k_i + 1125000)s + 1250k(e,r)k_i \quad (22)$$

When Routh tabulation is produced the following conditions are obtained for closed loop system stability:

Condition 1: If $k_p < 0$ and $0 < k_i \leq -\frac{k_p}{5}$ then $0 < k(e,r) < \rho(f(r(k_p, k_i)), \#1)$

Condition 2: If $k_p < 0$ and $-\frac{k_p}{5} < k_i < \rho(g_1(r(k_p, k_i)), \#3)$ then $0 < k(e,r) < \rho(f(r(k_p, k_i)), \#2)$

Condition 3: If $k_p < 0$ and $\rho(g_1(r(k_p, k_i)), \#3) < k_i < \rho(g_2(r(k_p, k_i)), \#4)$ then

$$0 < k(e,r) < \rho(f(r(k_p, k_i)), \#2) \text{ or } \rho(f(r(k_p, k_i)), \#3) < k(e,r) < \rho(f(r(k_p, k_i)), \#4)$$

Condition 4: If $k_p < 0$ and $k_i = \rho(g_2(r(k_p, k_i)), \#4)$ then $0 < k(e,r) < \rho(f(r(k_p, k_i)), \#2)$ or

$$\rho(f(r(k_p, k_i)), \#2) < k(e,r) < \rho(f(r(k_p, k_i)), \#4)$$

Condition 4: If $k_p < 0$ and $k_i > \rho(g_2(r(k_p, k_i)), \#4)$ then $0 < k(e,r) < \rho(f(r(k_p, k_i)), \#2)$

Condition 5: If $k_p \geq 0$ and $k_i > 0$ then $k(e,r) > 0$

Here, the notation $\rho(f(r)), \#n$ represents the smallest n^{th} root of $f(r)$ function, and limit polynomials are as follows

$$f(r(k_p, k_i)) = 1353026.88 + r(3808.54k_i + 1230768.8 k_p) + r^2(-10.2271 k_i^2 + 5796.14 k_i k_p + 90695.4 k_p^2) + r^3(0.020308 k_i^3 - 4.54447 k_i^2 k_p + 494.979 k_i k_p^2 + 999.255 k_p^3) + r^4(0.004 k_i^3 k_p + 0.0208 k_i^2 k_p^2 + 5.04 k_i k_p^3 + k_p^4) \quad (23)$$

$$g_1(r(k_p, k_i)) = 0.000276332 r^3 + 0.0468797r^2 k_p - 0.581928r k_p^2 + k_p^3$$

$$g_2(r(k_p, k_i)) = 7.96 \times 10^{-14} r^6 - 3.09 \times 10^{-11} r^5 k_p - 1.09 \times 10^{-8} r^4 k_p^2 + 7.9466 \times 10^{-6} r^3 k_p^3 - 0.0014 r^2 k_p^4 + 0.79 r k_p^5 - k_p^6$$

The results in previous section, in case of $k_p = -0.25$ and $k_i = 500$ and the case of $k_p = 12$ and $k_i = 150$ are examined. First case corresponds to 3rd condition, and the boundary for $k(e, r)$ is found as $0 < k(e, r) < 21.5675$. Second case corresponds to last condition, and the boundary for $k(e, r)$ is found as $k(e) > 0$.

In brief, using this criterion, the range of nonlinear gain $k(e, r)$ is determined by functions of k_p and k_i .

4.3. Stability Boundary Locus Method

In this case, the controller structure in (11) is used, and the function of k_p^* and k_i^* with respect to ω are computed as described in Section 3.3.

$$k_i^* = -\frac{7.01953125 \times 10^9 \omega^2 - 4.402886875 \times 10^7 \omega^4 + 45358.5 \omega^6 - 12.25 \omega^8}{(1 + 25 \omega^2)(1562500 - 2475 \omega^2 + \omega^4)} \tag{24}$$

$$k_p^* = -\frac{1406250000 + 4.9781875 \times 10^7 \omega^2 - 143454.375 \omega^4 + 126.925 \omega^6}{(1 + 25 \omega^2)(1562500 - 2475 \omega^2 + \omega^4)}$$

The stability boundary locus is plotted in the k_p - k_i plane by solving the equation set in Equation 24. Again, the line $k_i^* = 0$ is also the boundary of stability. The boundary locus plot for $\omega \in [0, 300]$ is given in Figure 15. The stable region in the plot is revealed by testing points in each region. As discussed in Section 3.3, the minimum value of $k(e, r)$ is 0, since k_i must be positive. Maximum value of $k(e, r)$ is calculated from the intersection point of boundary locus and the line that passing through the chosen (k_i, k_p) point and origin.

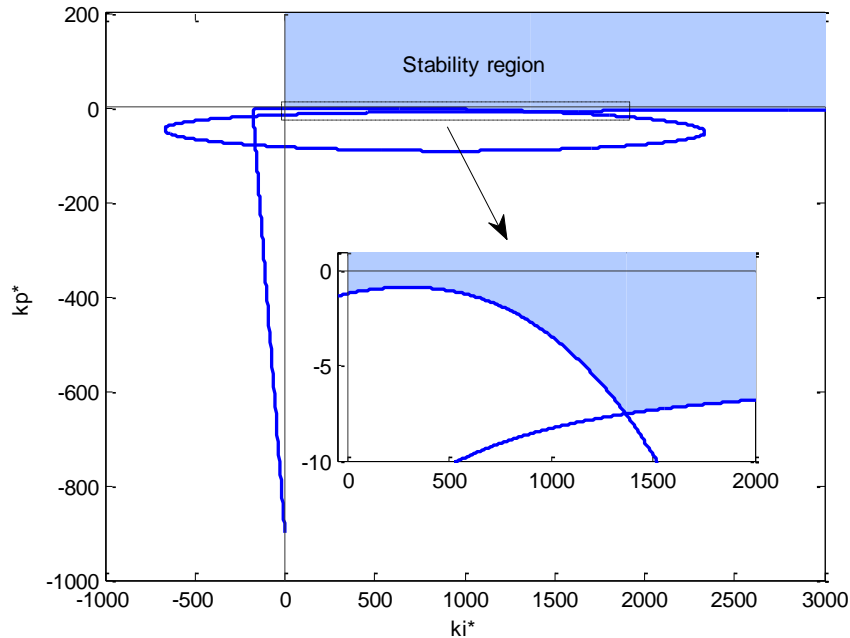


Figure 15. The stability boundary locus of active suspension system.

Again here, the case of $k_p = -0.25$ and $k_i = 500$ and the case of $k_p = 12$ and $k_i = 150$ are examined. For the first case, the (k_i^*, k_p^*) points are located on the straight line $k_p = -2000 k_i$. When this equation

In Figure 18, the close loop system response is presented with both the nonlinear PI and fixed-gain PI controller. It is observed that, the proposed controller is faster than the fixed-gain PI controller and also has less overshoot. In Figure 19, effects of α and γ variations on controller performance are examined while β is kept constant at 0.3. The results are similar with second order system results in Section 3.4, for small α values and large γ , system response accelerates.

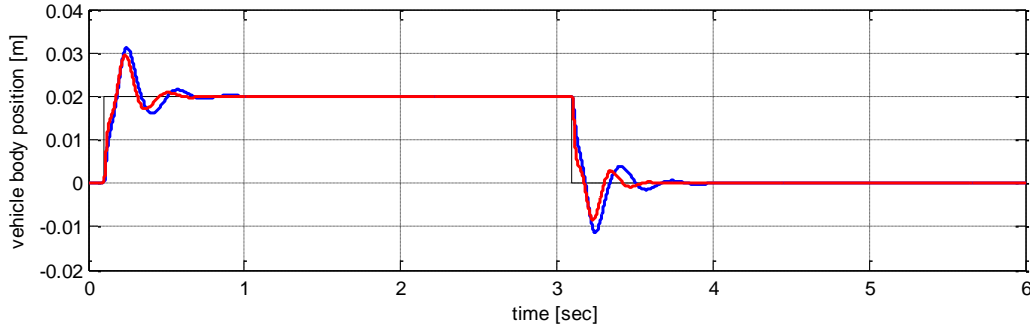


Figure 18. The closed loop system response. Road profile in black line, nonlinear PI controller response in red line, fixed-gain PI controller response in blue line.

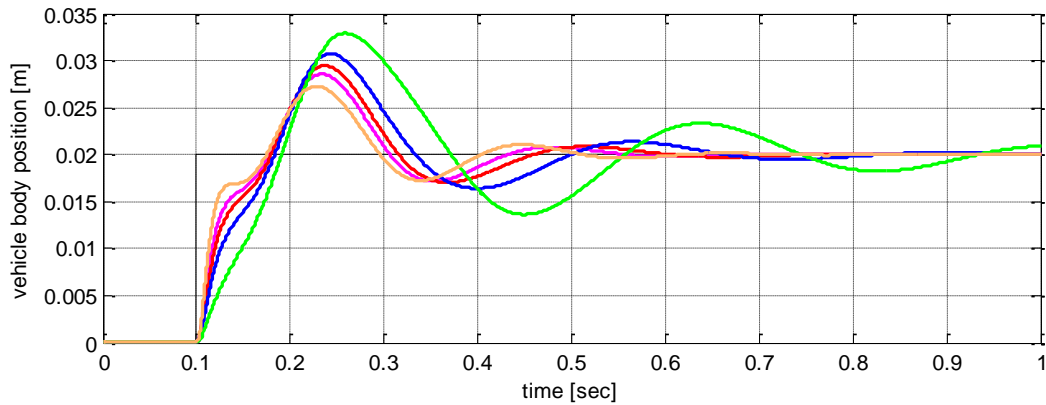


Figure 19. The controller performance for different parameters. Road profile in black line, $\alpha=0.1, \gamma=2$ in magenta line, $\alpha=1, \gamma=2$ in blue line, $\alpha=0.5, \gamma=1$ in green line, $\alpha=0.5, \gamma=3$ in orange line, nominal values in red line.

5. EXPERIMENTAL STUDIES

The proposed nonlinear PI controller is implemented for the active suspension system from Quanser[®] Consulting. It is a bench-scale model to emulate a quarter-car model controlled by an active suspension mechanism, see Figure 20. The upper mass (blue) represents the vehicle body supported above the suspension while the middle mass (red) corresponds to one of the vehicle's tires. The lower plate (silver) simulates the road surface by moving vertically. The upper mass is actuated through a controllable motor [22]. Manipulating the motor command force, control operation is performed. The parameters are listed as in Table 2. As controller parameters, same parameter set with simulations in the previous section is used.

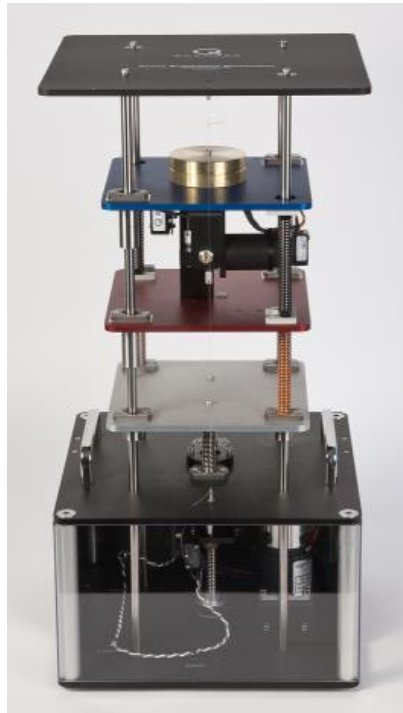


Figure 20. The active suspension system by Quanser [22].

In experiments, a square wave signal with 0.05 Hz and amplitude 0.02 is applied as the road profile. The open loop system response can be seen in Figure 21. The results of experiments are illustrated in Figure 22 and 23. As seen in Figure 22, although the proposed structure accelerates the system response, the overshoot is less as expected. In addition, the impact of integral term in steady state is more effective in case the proposed controller is used. When the effect of different α and γ values are examined, the similar results with simulations are observed (see Figure 23). Note that in Figure 23, the value of β is kept constant at 0.3.

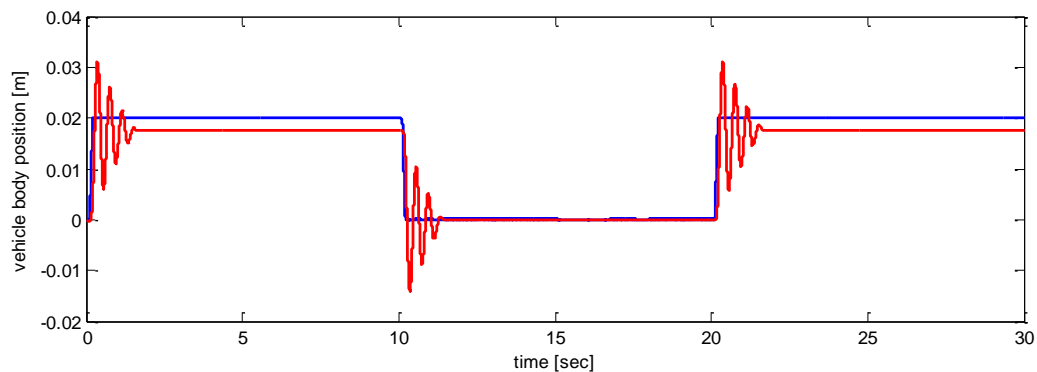


Figure 21. The open loop system response. Road profile in blue line, system response in red line.

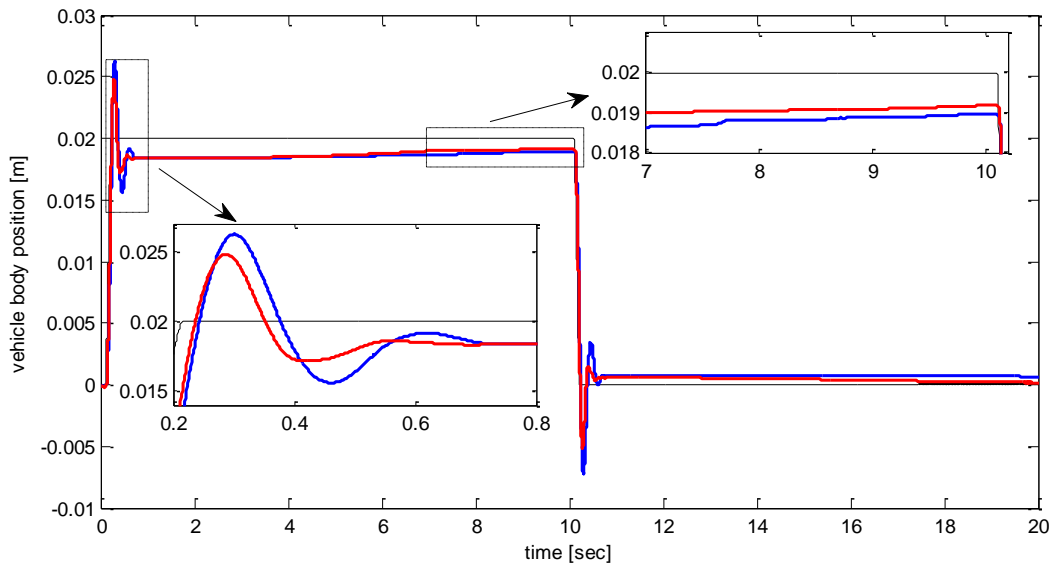


Figure 22. The closed loop system response. Road profile in black line, nonlinear PI controller response in red line, fixed-gain PI controller response in blue line.

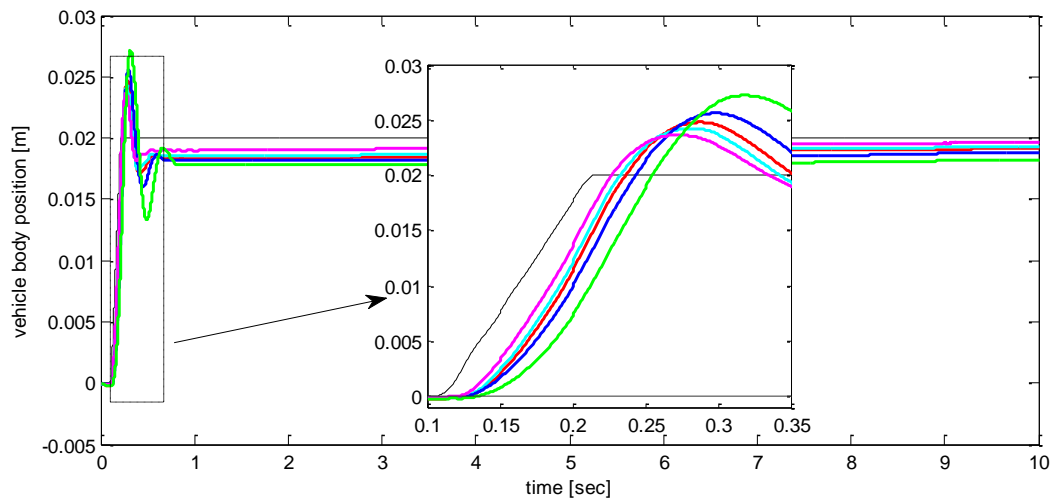


Figure 23. The controller performance for different parameters. Road profile in black line, $\alpha=0.1, \gamma=2$ in cyan line, $\alpha=1, \gamma=2$ in blue line, $\alpha=0.5, \gamma=1$ in green line, $\alpha=0.5, \gamma=3$ in magenta line, nominal values in red line.

6. CONCLUSION

In this paper, a novel nonlinear variable gain PI controller to improve the transient response of control systems is proposed. This new gain scheme increases the performance of even optimally designed fixed-gain controller introducing a nonlinear gain function of error and reference ratio. The range of nonlinear PI controller parameters that guarantee stability of the closed loop control system are investigated by three different methods for both second and higher order systems individually. Simulations are conducted to verify the performance of the proposed structure and found that the transient response is improved by reducing the tracking error with a satisfactory performance. The proposed controller is implemented on a vehicle active suspension system. Significant improvements of the transient response

are obtained experimentally in this case-study compared with the fixed-gain controller. In the proposed control scheme, only one nonlinear gain function is used for both proportional and integral part of the controller. In future work, asymmetric nonlinear gain functions will be used for each controller element including variable gain for differential term.

REFERENCES

- [1] Ang K, Chong G, Li Y. PID control system analysis, design, and technology, *IEEE Trans. Control Syst. Technol.*, vol. 13, no. 4, pp. 559–576, Jul. 2005.
- [2] Lau K, Middleton R. Switched integrator control schemes for integrating plants, in *Proc. Eur. Control Conf.*, 2003.
- [3] Hunnekens B G B, Heertjes M, van de Wouw N, Nijmeijer H. Performance optimization of piecewise affine variable-gain controllers for linear motion systems, *Mechatronics*, vol. 24, no. 6, pp. 648–660, Sep. 2014.
- [4] Armstrong B, Neevel D, Kusik T. New results in NPID control: Tracking, integral control, friction compensation and experimental results, *IEEE Trans. Contr. Syst. Technol.*, vol. 9, pp. 399–406, Mar. 2001.
- [5] Hunnekens B G B, Heertjes M, van de Wouw N, Nijmeijer H. Synthesis of variable gain integral controllers for linear motion systems, *IEEE Trans. on Contr. Syst. Technology*, 23(1), pp. 139-149, 2015.
- [6] Armstrong B., McPherson J., and Li Y. Stability of nonlinear PD control, *Appl. Math. Comput. Sci.*, vol. 7, no. 2, pp. 101–120, 1997.
- [7] Armstrong B., Neevel D., and Kusik T. New results in NPID control: Tracking, integral control, friction compensation and experimental results, in *Proc. 1999 Int. Conf. Robot. Automat.*, 1999, pp. 837–842.
- [8] Armstrong B. and Wade B. Nonlinear PID control with partial state knowledge: Damping without derivatives, *Int. J. Robot. Res.*, vol. 18, no. 8, pp. 715–731, 2000.
- [9] Armstrong B, Neevel D, Kusik T. New results in NPID control: Tracking, integral control, friction compensation and experimental results, *IEEE Trans. Control Syst. Technol.*, vol. 9, no. 2, pp. 399–406, Mar. 2001.
- [10] Heertjes M, Schuurbiers X, Nijmeijer H. Performance-improved design of N-PID controlled motion systems with application to wafer stages, *IEEE Trans. Ind. Electron.*, vol. 56, no. 5, pp. 1347–1355, May 2009.
- [11] Wouw N, Pastink H, Heertjes M, Pavlov A, Nijmeijer H. Performance of convergence-based variable-gain control of optical storage drives, *Automatica*, vol. 44, no. 1, pp. 15–27, 2008.
- [12] Sun D, Hu S, Shao X, Liu C. Global stability of a saturated nonlinear PID controller for robot manipulators, *IEEE Trans. Ind. Electron.*, vol. 17, no. 4, pp. 892–899, Jul. 2009.
- [13] Salim S N S, Rahmat M F, Faudzi A A, Athif M, Ismail Z H, Sunar N. Position Control of Pneumatic Actuator Using Self-Regulation Nonlinear PID, *Mathematical Problems in Engineering*, vol. 2014, p. 12, 2014

- [14] Seraji H. A new class of nonlinear PID controllers with robotic applications, *J. Robot. Syst.*, vol. 15, no. 3, pp. 161–173, 1998.
- [15] Su Y X, Sun D, Duan B Y. Design of an enhanced nonlinear PID controller, *Mechatronics*, vol. 15, no. 8, pp. 1005–1024, Oct. 2005.
- [16] Salim S N S, Rahmat M F, Faudzi A, Z. Ismail Z H, Sunar N. Robust Control Strategy for Pneumatic Drive System via Enhanced Nonlinear PID Controller, *International Journal of Electrical and Computer Engineering (IJECE)*, vol. 4, pp. 658-667, 2014.
- [17] Armstrong B, McPherson J, Li YG. A Lyapunov stability proof for nonlinear stiffness PD control, *Proceedings of the IEEE international conference on robot. autom.*, Minneapolis, p. 945–50, 1996.
- [18] Xu Y, Ma D, Hollerbach J. M. Nonlinear Proportional and Derivative Control for High Disturbance Rejection and High Gain Force Control, *Proc. IEEE Intern. Conf. on Robotics and Automation*, Vol. 1, pp. 752-759, Atlanta, 1993.
- [19] Tan, N, Kaya, I, Yeroglu C, Atherton, D. P. Computation of stabilizing PI and PID controllers using the stability boundary locus. *Energy Conversion and Management*, 47(18), 3045-3058.
- [20] Yeroglu C, Tan N. Design of robust PI controller for vehicle suspension system. *Journal of Electrical Engineering and Technology*, 3(1), 135-142.
- [21] Khalil H K, Grizzle J. *Nonlinear Systems*, 3rd ed. Englewood Cliffs, NJ, USA: Prentice-Hall, 2002.
- [22] *Active suspension system - Laboratory Guide, Active Suspension Experiment for Matlab/Simulink Users*, 2013.